Journal of ELECTRONIC MATERIALS, Vol. 41, No. 4, 2012
DOI: 10.1007/s11664-012-1921-0
© 2012 TMS

Effect of Pd Thickness on the Interfacial Reaction and Shear Strength in Solder Joints Between Sn-3.0Ag-0.5Cu Solder and Electroless Nickel/Electroless Palladium/Immersion Gold (ENEPIG) Surface Finish

YOUNG MIN KIM,[1] JIN-YOUNG PARK,[1] and YOUNG-HO KIM[1,2]

1.—Division of Materials Science & Engineering, Hanyang University, Seoul 133-791, Korea.
2.—e-mail: kimyh@hanyang.ac.kr

Intermetallic compound formation at the interface between Sn-3.0Ag-0.5Cu (SAC) solders and electroless nickel/electroless palladium/immersion gold (ENEPIG) surface finish and the mechanical strength of the solder joints were investigated at various Pd thicknesses (0 μm to 0.5 μm). The solder joints were fabricated on the ENEPIG surface finish with SAC solder via reflow soldering under various conditions. The $(Cu,Ni)_6Sn_5$ phase formed at the SAC/ENEPIG interface after reflow in all samples. When samples were reflowed at 260°C for 5 s, only $(Cu,Ni)_6Sn_5$ was observed at the solder interfaces in samples with Pd thicknesses of 0.05 μm or less. However, the $(Pd,Ni)Sn_4$ phase formed on $(Cu,Ni)_6Sn_5$ when the Pd thickness increased to 0.1 μm or greater. A thick and continuous $(Pd,Ni)Sn_4$ layer formed over the $(Cu,Ni)_6Sn_5$ layer, especially when the Pd thickness was 0.3 μm or greater. High-speed ball shear test results showed that the interfacial strengths of the SAC/ENEPIG solder joints decreased under high strain rate due to weak interfacial fracture between $(Pd,Ni)Sn_4$ and $(Cu,Ni)_6Sn_5$ interfaces when the Pd thickness was greater than 0.3 μm. In the samples reflowed at 260°C for 20 s, only $(Cu,Ni)_6Sn_5$ formed at the solder interfaces and the $(Pd,Ni)Sn_4$ phase was not observed in the solder interfaces, regardless of Pd thickness. The shear strength of the SAC/ENIG solder joints was the lowest of the joints, and the mechanical strength of the SAC/ENEPIG solder joints was enhanced as the Pd thickness increased to 0.1 μm and maintained a nearly constant value when the Pd thickness was greater than 0.1 μm. No adverse effect on the shear strength values was observed due to the interfacial fracture between $(Pd,Ni)Sn_4$ and $(Cu,Ni)_6Sn_5$ since the $(Pd,Ni)Sn_4$ phase was already separated from the $(Cu,Ni)_6Sn_5$ interface. These results indicate that the interfacial microstructures and mechanical strength of solder joints strongly depend on the Pd thickness and reflow conditions.

Key words: Pb-free solder, ENEPIG, Pd thickness, interfacial microstructure, mechanical strength

INTRODUCTION

Electroless nickel/immersion gold (ENIG) is the most common electroless method for creating surface finishes for Pb-free solders used in microelectronic packaging industries due to the low-cost plating process, slow intermetallic compound (IMC) growth rate, and good solder-wetting behavior.[1] Although ENIG exhibits good reliability improvement, the production cost is relatively high due to the thick Au layer.[2] In addition, galvanic hyper corrosion in the

(Received August 25, 2011; accepted January 5, 2012; published online February 23, 2012)

Ni(P) layer caused by immersion in a gold solution can result in the formation of Ni oxides on the Ni(P) surface, which reduces the reliability of the solder joints.[3–6] This black pad problem has been one of the critical issues in packaging industries. To overcome the weak solder joint reliability issues in ENIG, an electroless nickel/electroless palladium/immersion gold (ENEPIG) trilayer structure has been developed by introducing a Pd layer between the Ni and Au bilayer.[7–9] As a result, corrosion is significantly reduced on the Ni(P) layer during the Pd plating process. Other advantages of the Pd layer include lower production cost and greater compatibility with wire-bonding processes.[4] In addition, electromigration-induced Ni(P) consumption and electromigration-induced diffusion of the IMC layer were effectively retarded at the solder/ENEPIG interfaces.[10]

However, studies investigating the effect of Pd thickness on the interfacial reaction between Sn-Ag-Cu (SAC) solder alloys and ENEPIG are still seriously lacking. Previous studies used a narrow Pd thickness range from 0.05 μm to 0.3 μm for reflow soldering applications.[5–8] The growth of $(Cu,Ni)_6Sn_5$ formed at the solder/Ni(P) interface was retarded by the introduction of an additional Pd layer between the Ni and Au layers, and the mechanical strengths of the SAC/ENEPIG solder joints were improved compared with that of the ENIG surface finish.[6,11,12] However, the effects of Pd thickness on the mechanical strength and the optimum Pd thickness exhibited disparities in previous studies.[5–8] These disparities may be due to the different reflow conditions which result in the evolution of different interfacial microstructures.

In this study, the effect of Pd thickness on the interfacial reaction between the ENEPIG surface finish and SAC solder was investigated by varying the thickness of Pd from 0 μm to 0.5 μm and using various reflow conditions. In addition, to investigate the correlation of mechanical properties with interfacial microstructures, the high-speed ball shear test was performed at a range of shear speeds based on the Joint Electronic Device Engineering Council (JEDEC) solder ball shear test standard JESD22-B117.[13]

EXPERIMENTAL PROCEDURES

The composition of the ball grid array solder balls used in this study was Sn-3.0Ag-0.5Cu (in wt.%, SAC), and their diameters were 760 μm. The substrate was bismaleimide triazine (BT) printed circuit board surrounded by a solder mask with pad opening of 650 μm diameter that was used for attachment to the solder ball. The surface finish, electroless Ni/Pd/Au, was deposited on Cu bond pads. The thicknesses of the Au and Ni(P) layers were 0.15 μm and 5 μm, respectively. The thickness of the electroless plated Pd layer decreased during the immersion Au plating because of the replacement reaction between Pd and Au atoms, thus the thickness of the Pd layer was adjusted considering the Pd consumption. The final Pd thickness was varied from 0 μm (i.e., ENIG) to 0.5 μm. The solder balls were joined to the pads of BT substrates in a reflow process using a water-soluble halide-free flux in a convection reflow oven. In previous studies, the reflow soldering of SAC solders was performed at a peak temperature of 260°C, and the time above the melting point of SAC (dwell time) was 90 s.[5–8] In our study, the peak temperature was set to 260°C and the holding time at peak temperature was 5 s (dwell time 85 s) or 20 s (dwell time 100 s). The interfacial IMCs and microstructure of the solder joints after reflow were analyzed using scanning electron microscopy (SEM) with energy-dispersive spectroscopy (EDS). Phase compositions and elemental mapping analyses were characterized by field-emission electron probe microanalyzer (FE-EPMA, JEOL JXA-8500F). Due to the nonuniform thickness of the IMC layer, such as those of the $(Cu,Ni)_6Sn_5$ and $(Pd,Ni)Sn_4$ phases, the average thickness of the IMC layers was calculated by dividing the total area of the IMCs by the length of the interface of the cross-sectional images. A ball shear test was performed on the as-reflowed samples using a DAGE-4000HS bond tester. The test was performed under displacement control and at various displacement rates (10 mm/s, 100 mm/s, 500 mm/s, and 1000 mm/s) at shear height of 50 μm from the surface of the substrate. In each test condition, the shear test was repeated more than 30 times. The fracture surface after the shear test was analyzed using SEM.

RESULTS AND DISCUSSION

Interfacial Microstructure of the SAC/ENEPIG Under Various Reflow Conditions

First, the interfacial microstructures were investigated under various reflow conditions when the Pd thickness was 0.5 μm. The SAC/ENEPIG solder joints were reflowed at 255°C, 260°C, and 265°C for 5 s, 10 s, and 20 s, respectively. Figure 1 depicts back-scattered electron (BSE) micrographs of the solder joint interfaces. When the samples were reflowed at 255°C for 5 s, as seen in Fig. 1a, an unreacted Pd layer was observed above Ni(P), and a continuous and thick ternary Pd-Ni-Sn phase formed on the Pd layer at the interface. The composition of this phase was determined to be 15.61 at.% to 17.54 at.% Pd, 1.43 at.% to 3.24 at.% Ni, and 79.67 at.% to 82.96 at.% Sn according to wavelength-dispersed spectroscopy (WDS). The composition of this phase, similar to previous results,[9,14–16] was identified as $(Pd,Ni)Sn_4$. As the reflow holding time increased to 10 s, Pd was totally consumed during the reaction with Sn and the thickness of the $(Pd,Ni)Sn_4$ phase increased. Also, $(Pd,Ni)Sn_4$ was partially spalled from the interface and thin $(Cu,Ni)_6Sn_5$ IMC formed at the SAC/ENEPIG interface. When the reflow holding time was prolonged to 20 s, detached $(Pd,Ni)Sn_4$ was rarely observed in the solder

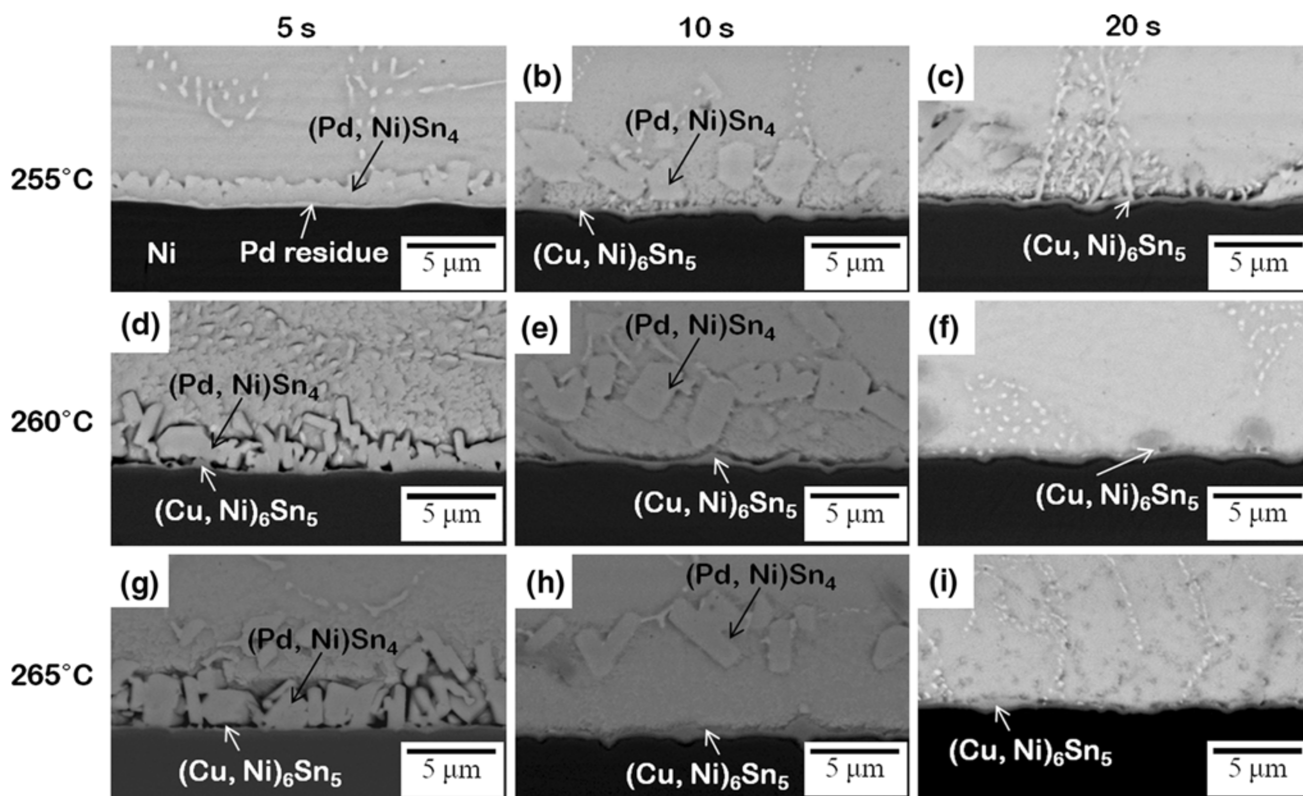

Fig. 1. BSE micrographs of the SAC/ENEPIG interfaces (Pd: 0.5 μm) under various reflow conditions.

interface and only a thin $(Cu,Ni)_6Sn_5$ phase was observed at the solder interface. When specimens were reflowed at 260°C for 5 s, partially spalled $(Pd,Ni)Sn_4$ and thin $(Cu,Ni)_6Sn_5$ layers were formed and no Pd layer was observed. The composition of the $(Pd,Ni)Sn_4$ phase was 13.5 at.% to 14.1 at.% Pd, 4.6 at.% to 5.3 at.% Ni, and 80.2 at.% to 80.5 at.% Sn. $(Cu,Ni)_6Sn_5$ and $(Pd,Ni)Sn_4$ IMCs were observed near the solder interface after reflow for 10 s, and most of the $(Pd,Ni)Sn_4$ layer was detached from the interface. The tendency for detachment of the $(Pd,Ni)Sn_4$ phase from the solder joint interfaces was accelerated as the reflow holding time increased. When the reaction time was prolonged to 20 s (Fig. 1f), the continuous $(Pd,Ni)Sn_4$ phase was not observed near the solder interfaces due to the spalling of $(Pd,Ni)Sn_4$. As the reflow temperature increased to 265°C, the detachment of the $(Pd,Ni)Sn_4$ was observed after reflow holding time of 5 s. Thin $(Cu,Ni)_6Sn_5$ IMC formed beneath the $(Pd,Ni)Sn_4$ as presented in Fig. 1g. For the reflow condition of 265°C for 10 s, complete separation of the $(Pd,Ni)Sn_4$ layer from the solder interface was observed, as seen in Fig. 1h. After reflowing at 265°C for 20 s, no $(Pd,Ni)Sn_4$ phase remained near the solder interface, as shown in Fig. 1i. Only thin $(Cu,Ni)_6Sn_5$ layer was observed when the $(Pd,Ni)Sn_4$ IMC detached from the solder interface, as shown in Fig. 1b, c, e, f, h, i.

Generally, a regular spalling phenomenon occurs when the solder-wettable layer of the under bump metallurgy or substrate metallurgy is completely exhausted.[17–19] This is unlike the situation encountered in this study, where most of the $(Pd,Ni)Sn_4$ spalled from the solder interface, even though the solder-wettable Ni(P) layer had not yet been consumed. A similar phenomenon of spalling of $(Pd,Ni)Sn_4$ from the solder interface was reported in the interfacial reaction between SAC and ENEPIG surface finish,[8,16] although the Pd thickness in that ENEPIG was not the same as in this study. The detachment of $(Pd,Ni)Sn_4$ from the interface reflects the instability of the interface between $(Pd,Ni)Sn_4$ and $(Cu,Ni)_6Sn_5$. The thick $(Pd,Ni)Sn_4$ layer imposes stress in the interface and is easily separated during reflow. The convection of molten solder and the low-density $PdSn_4$ compared with Sn may also help the detachment of $(Pd,Ni)Sn_4$ from the $(Cu,Ni)_6Sn_5$ interface.[20] As seen in Fig. 1, the interfacial microstructure at the SAC/ENEPIG was very sensitive to the reflow temperature and holding times. Two reflow conditions of 260°C for 5 s and 20 s were chosen to produce two distinctive interfacial microstructures that allowed evaluation of the effect of Pd thickness on the interfacial reaction and interfacial strengths of the solder joints.

Interfacial Reaction and Strengths of SAC/ENEPIG Solder Joints After Reflow at 260°C for 5 s

Figure 2 depicts cross-sectional BSE micrographs of the SAC/ENEPIG interfaces with Pd layers of

various thicknesses reflowed above 260°C for 5 s. In the as-reflowed condition, no meaningful Au signals were detected in the SAC solder joints in all samples, since the thin Au layer (0.15 μm) dissolved completely into the solder matrix once the solder was molten. A residual Pd layer was not observed at the SAC/ENEPIG solder interfaces in this reflow condition, regardless of Pd thickness. This result is consistent with the interfacial microstructures exhibited in Fig. 1d. For the ENIG surface finish, a single IMC layer of $(Cu,Ni)_6Sn_5$ with many polygonal rods was observed at the interfaces after reflow. The $(Cu,Ni)_6Sn_5$ was composed of 20.3 at.% Ni, 34.6 at.% Cu, and 45.1 at.% Sn, where Ni is dissolved into the Cu sublattice.[21] The formation of $(Cu,Ni)_6Sn_5$ rather than Ni_3Sn_4 at the SAC/Ni(P) interface can be explained through the local equilibrium correlation between Ni and the solders, when the Cu concentration is equal to or greater than 0.5 wt.%.[22,23]

At Pd thickness of 0.05 μm, a $(Cu,Ni)_6Sn_5$ phase formed and $(Pd,Ni)Sn_4$ was not observed at the solder interfaces. Pd atoms dissolved into the molten solder and reacted with Ni atoms that diffused from the Ni(P) layer, which resulted in the formation of $(Pd,Ni)Sn_4$ as a precipitation product when the Pd thickness exceeded 0.1 μm at an early stage of reflow.[5–8] As the Pd thickness increased, the discontinuous particle-like $(Pd,Ni)Sn_4$ phase changed to a continuous $(Pd,Ni)Sn_4$ layer over the $(Cu,Ni)_6Sn_5$ phase and this IMC significantly thickened.

Figures 3 and 4 show FE-EPMA elemental mapping images of the very thin (0.05 μm) and thick (0.5 μm) Pd thicknesses of the samples shown in Fig. 2. Secondary-electron (SE) and BSE images are presented in both figures. These elemental mapping images provide a more detailed microstructure and elemental distribution in the reaction zone. Two distinct layers were clearly observed between the $(Cu,Ni)_6Sn_5$ IMC and the electroless Ni-P by combining the Ni, P, and Sn elemental mapping images in Figs. 3 and 4, which were confirmed to be Ni_3P and nanocrystalline ternary Ni-Sn-P compound layers, respectively.[24,25] The P atoms were rejected, and a P-rich layer formed beneath the IMCs, which crystallized to form a crystalline Ni_3P layer.[24] The ternary Ni-Sn-P phase was the result of a reaction between the P-rich Ni phase and internally diffused Sn because the ternary Ni-Sn-P phase was formed at the uppermost region of the P-rich Ni phase.[25] According to Fig. 3, elemental Pd was not detected and only $(Cu,Ni)_6Sn_5$ was observed at the SAC/ENEPIG interface, indicating that the very thin Pd layer was totally dissolved into the solder. In contrast, a thick and discontinuous $(Pd,Ni)Sn_4$ phase formed on the $(Cu,Ni)_6Sn_5$, as seen in Fig. 4. Pd

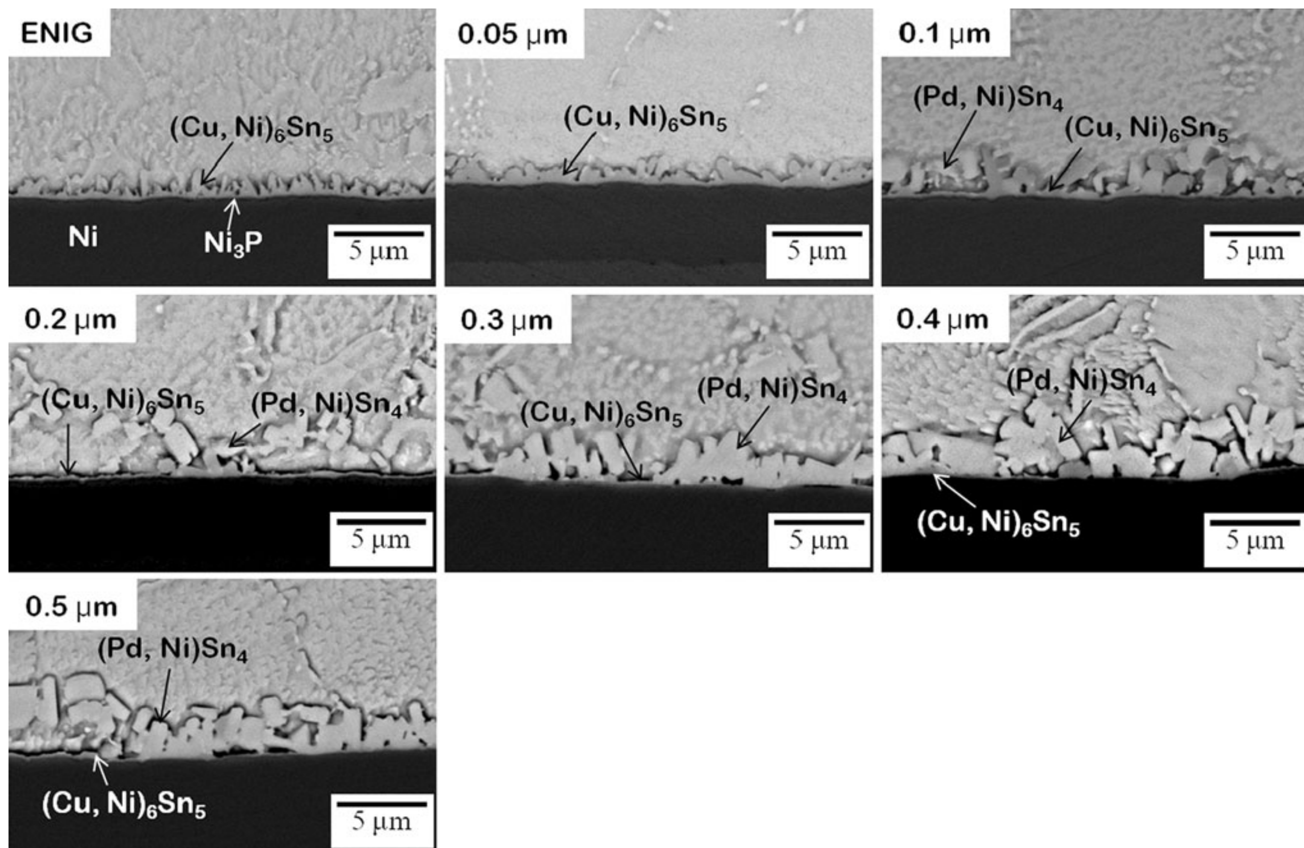

Fig. 2. BSE micrographs of the SAC/ENEPIG interfaces with different thicknesses of Pd reflowed above 260°C for holding time of 5 s.

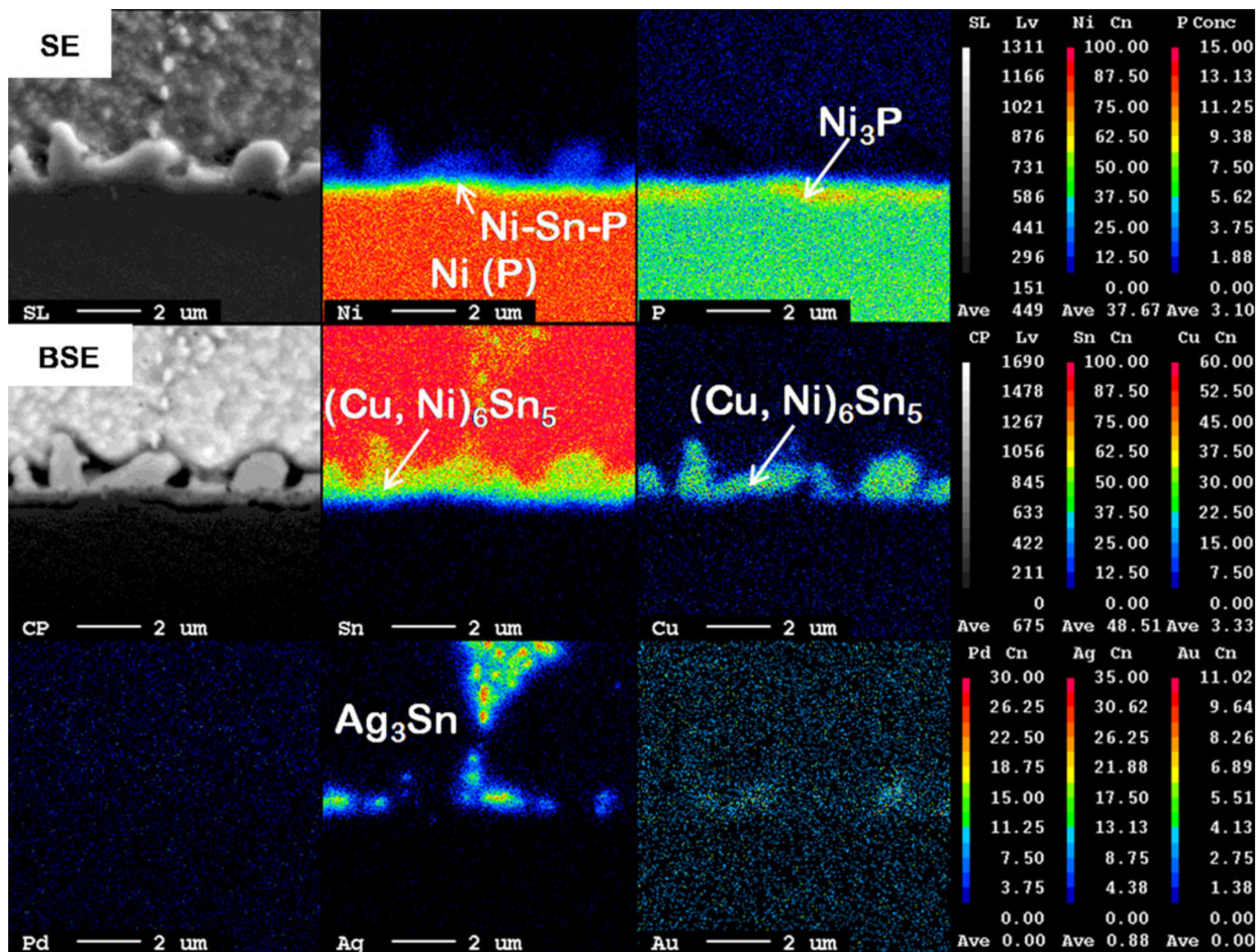

Fig. 3. FE-EPMA elemental mapping of Ni, P, Sn, Cu, Pd, Ag, and Au x-rays at the SAC/ENEPIG interface with Pd thickness of 0.05 μm.

atoms were detected in the $(Cu,Ni)_6Sn_5$ IMC, and the Pd composition in this IMC was about 3.5 at.%, which suggests that a small amount of Pd atoms had been incorporated into the $(Cu,Ni)_6Sn_5$ phase after reflow. The Ni content in the $(Cu,Ni)_6Sn_5$ formed in the 0.5 μm Pd sample was lower than that in the 0.05 μm Pd specimen. A similar trend was reported for the Ni content, which decreased at the interfaces as the Pd thickness increased.[8] This result could be ascribed to depletion of Ni atoms in $(Cu,Ni)_6Sn_5$ to form a Ni-containing $(Pd,Ni)Sn_4$ phase since $(Pd,Ni)Sn_4$ is more stable than $PdSn_4$.[20]

Based on Fig. 2, the average thicknesses of the $(Cu,Ni)_6Sn_5$, $(Pd,Ni)Sn_4$, and overall IMCs were plotted with respect to Pd thickness, as seen in Fig. 5. The overall IMC thickness increased as the Pd thickness increased. The thickness of the $(Pd,Ni)Sn_4$ IMC proportionally increased with Pd thickness when the Pd thickness was greater than 0.1 μm. The main contribution to the overall IMC growth was the increase in the thickness of the $(Pd,Ni)Sn_4$ phase. On the contrary, when the Pd thickness was 0.05 μm, the $(Cu,Ni)_6Sn_5$ thickness increased only slightly compared with that of the ENIG surface finish. This behavior was very similar to a previous study using the same Pd thickness.[26] The Pd layer addition resulted in accelerated IMC growth at an early reflow stage. The thickness of $(Cu,Ni)_6Sn_5$ gradually decreased as the Pd thickness increased. This thick and continuous $(Pd,Ni)Sn_4$ that formed over the $(Cu,Ni)_6Sn_5$ IMC played a role as a diffusion barrier between Sn and Ni (and Cu) atoms and retarded the formation and growth of $(Cu,Ni)_6Sn_5$ during the reflow.[11,12]

To evaluate the mechanical strengths of the solder joints with various interfacial microstructures derived from various Pd thicknesses, the ball shear test was used under various shear speeds. Figure 6 depicts the shear strength variation of the SAC/ENEPIG solder joints that formed after reflow for 5 s with different Pd thicknesses under various shear speeds. Increasing shear speed generally increased the shear strength in the samples of the thin Pd layers (0 μm to 0.2 μm), leading higher strength of solder by work hardening effect.[27,28] At low shear speeds such as 10 mm/s or 100 mm/s, the shear strength values of the SAC/ENEPIG solder joints were almost equal to one another, regardless

Fig. 4. FE-EPMA elemental mapping of Ni, P, Sn, Cu, and Pd x-rays at the SAC/ENEPIG interface with Pd thickness of 0.5 μm.

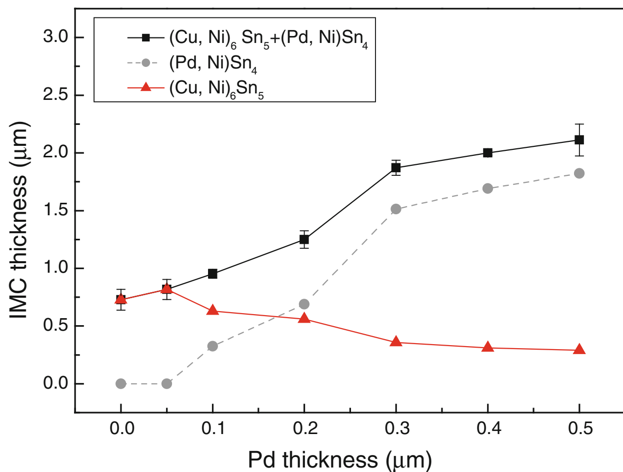

Fig. 5. Thickness of IMCs after reflow at 260°C as a function of Pd thickness for the total IMCs, $(Cu,Ni)_6Sn_5$, and $(Pd,Ni)Sn_4$ under reflow condition for 5 s.

of Pd thickness. For shear speed of 500 mm/s, the shear strength of the solder joints substantially decreased for Pd thickness of 0.5 μm. In addition, the shear strength decreased significantly with increasing Pd thickness above 0.3 μm at shear speed of 1000 mm/s.

Figure 7 depicts representative fracture surface micrographs on the pad side after high-speed ball shear tests. The failure modes were classified into five modes (ductile, quasiductile, quasibrittle, brittle, and pad lift). Three characteristic fracture modes were ductile fracture following solder (Fig. 7a), brittle fracture at the solder/IMC or IMC/IMC interface (Fig. 7d), and pad lift in which the Cu trace delaminated from the BT substrate (Fig. 7e). To clarify the discrimination of the qualitative failure mode assessments,[29] mixed ductile/brittle modes were divided into two classifications: quasiductile (>50% ductile mode, Fig. 7b) and quasibrittle (>50% brittle mode, Fig. 7c).

Figure 8 shows detailed views of the two different brittle fractured surfaces after high-speed ball shear tests. Both fractographs in Fig. 8a, b show the $(Cu,Ni)_6Sn_5$ intermetallic surfaces. The morphology of the $(Cu,Ni)_6Sn_5$ IMC formed on ternary Ni–Sn-P was quite variable with respect to Pd thickness, as seen in Fig. 8. For Pd thickness of 0.3 μm or greater,

the grain size of $(Cu,Ni)_6Sn_5$ IMC was much finer than that formed in SAC/ENEPIG solder joints with Pd thickness of 0.2 μm or less, since growth of the $(Cu,Ni)_6Sn_5$ phase was suppressed by the formation of a continuous $(Pd,Ni)Sn_4$ layer. When the Pd thickness was 0.2 μm or less, fractures occurred along the solder/$(Cu,Ni)_6Sn_5$ interfaces, as shown in Fig. 8a. However, for Pd thickness of 0.3 μm or more, the main fractures occurred at the interface between the $(Pd,Ni)Sn_4$ and $(Cu,Ni)_6Sn_5$ layers, as shown in Fig. 8b. Since the crack propagated through the $(Pd,Ni)Sn_4$/$(Cu,Ni)_6Sn_5$ interface, only $(Cu,Ni)_6Sn_5$ IMC was observed at the fractured surface. The shear strength results for the SAC/ENEPIG solder joints and the fractured surface presented in Figs. 6 and 8 imply that the crack propagated more easily at the $(Pd,Ni)Sn_4$/$(Cu,Ni)_6Sn_5$ interface compared with at the solder/$(Cu,Ni)_6Sn_5$ interface.

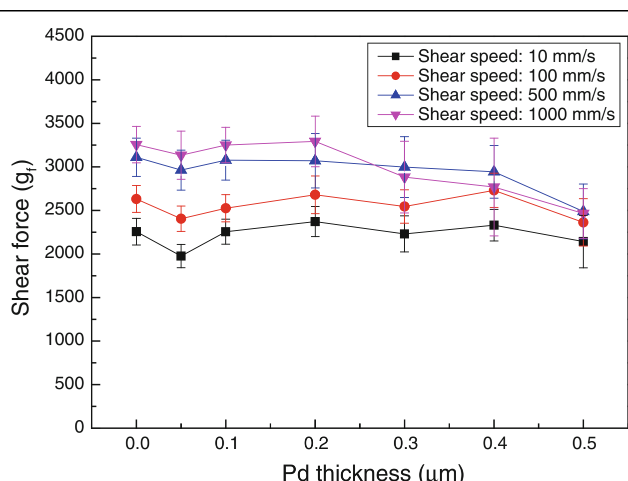

Fig. 6. Shear strength variation of SAC/ENEPIG under different thicknesses of Pd with various shear speeds after reflow for 5 s.

The failure mode distributions after the high-speed ball shear test of SAC/ENEPIG solder joints with various Pd thicknesses fabricated with reflow temperature at 260°C for 5 s under different shear speeds are shown in Fig. 9. For slow strain rate at shear speed of 10 mm/s, all failure modes were ductile fractures which occurred in the solder region. As the shear speed increased to 100 mm/s, small fractions of quasiductile, quasibrittle, and pad lift modes were observed in the Pd thickness ranges from 0 μm to 0.05 μm and 0.4 μm to 0.5 μm. This suggests that the ball shear test performed under slow shear speeds did not reflect a significant difference in the fracture mode analysis, irrespective of the Pd thickness. At high strain rate of 500 mm/s or 1000 mm/s, quasiductile, quasibrittle, and brittle modes were more frequently observed compared with at slow shear speed conditions. When the Pd layer in the ENEPIG was thick, a $(Pd,Ni)Sn_4$/$(Cu,Ni)_6Sn_5$ bilayer formed at the solder interface.

When the loading speed increased, the solder needed to accommodate a high strain rate. Since the resistance to the deformation of the solder material increases with strain rate, high stresses are built up at the joint interfaces. Under these conditions, the solder joint interfaces can become the weakest link in the structures, and interface failure occurs.[30] Interfacial fractures that propagated between

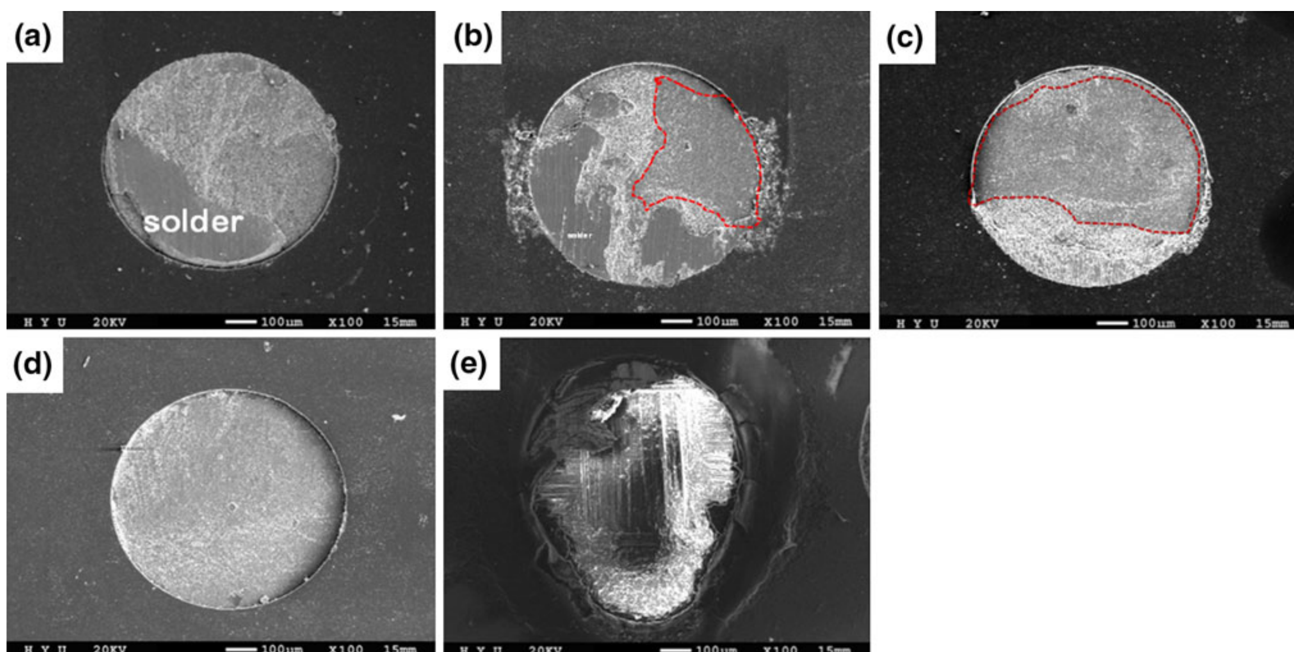

Fig. 7. High-speed ball shear failure modes: (a) ductile mode (100% area with solder left), (b) quasiductile mode (>50% ductile mode), (c) quasibrittle mode (>50% brittle mode), (d) brittle mode (almost no solder left), and (e) pad lift with brittle.

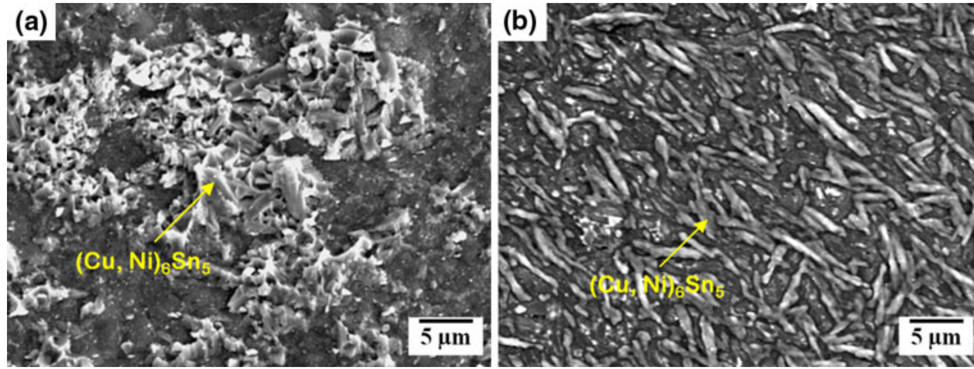

Fig. 8. Typical fractography of SAC/ENEPIG solder joints formed at 260°C for 5 s in brittle mode after high-speed shear testing: (a) Pd thickness ≤0.2 μm and (b) Pd thickness ≥0.3 μm.

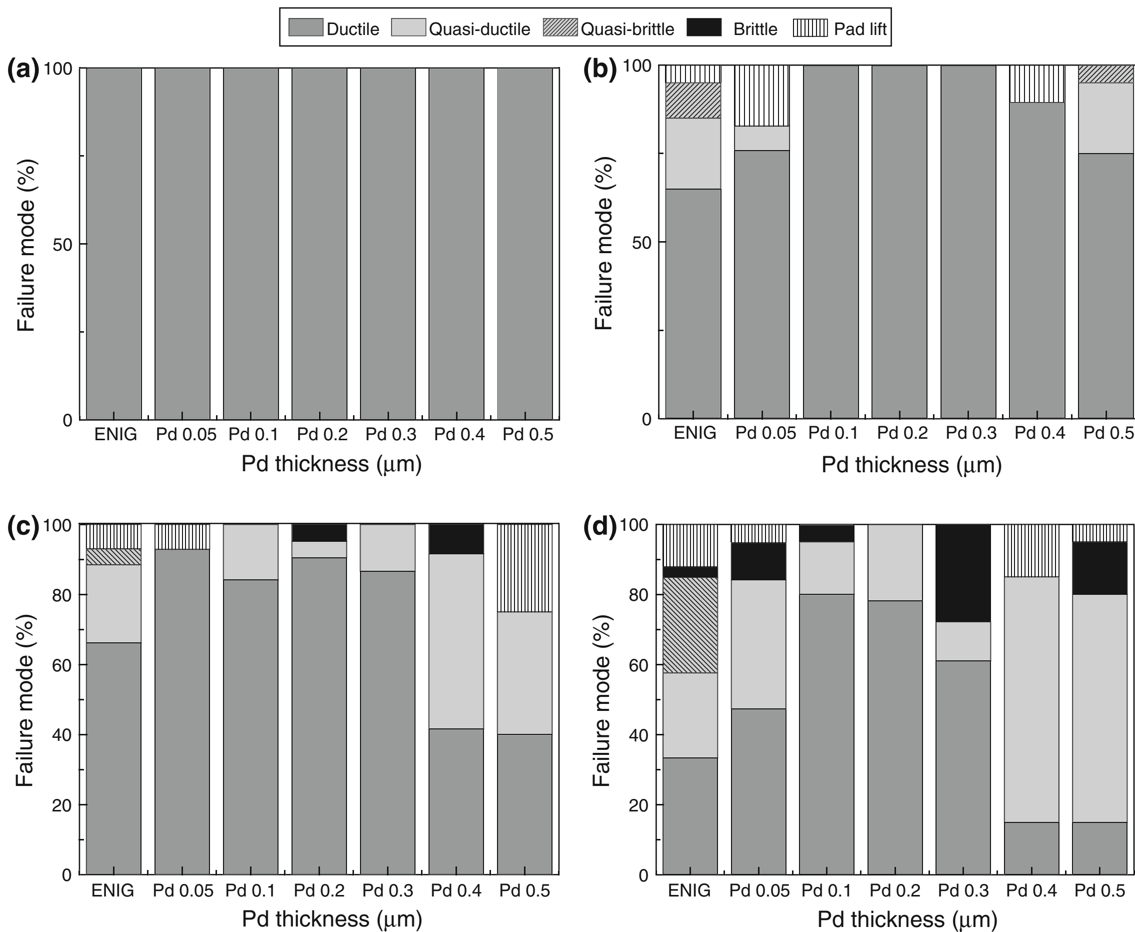

Fig. 9. Failure mode distribution after ball shear test of SAC/ENEPIG solder joints with different thicknesses of Pd under various shear speeds (reflow holding time: 5 s): (a) 10 mm/s, (b) 100 mm/s, (c) 500 mm/s, and (d) 1000 mm/s.

bilayers of the IMCs were often observed due to crack propagation through the IMC/IMC interfacial path under dynamic loading. It is well known that the mechanical strength is degraded when (Au,-Ni)Sn_4 is formed on Ni_3Sn_4[5,6,14] or (Cu,Ni)$_6$Sn$_5$,[31] similar to that observed in our study. It has been reported that the interfacial strength dramatically decreased in Pd-containing solder/Ni solder joints when the Pd concentration in the solder was greater than 0.2 wt.%, and the fractures mainly occurred at the (Pd,Ni)Sn_4/Ni_3Sn_4 interface.[32] Due to the formation of the (Pd,Ni)Sn_4 phase, brittle fractures occurred more frequently because the (Pd,Ni)Sn_4/(Cu,Ni)$_6$Sn$_5$ interface in the solder joints was weak.

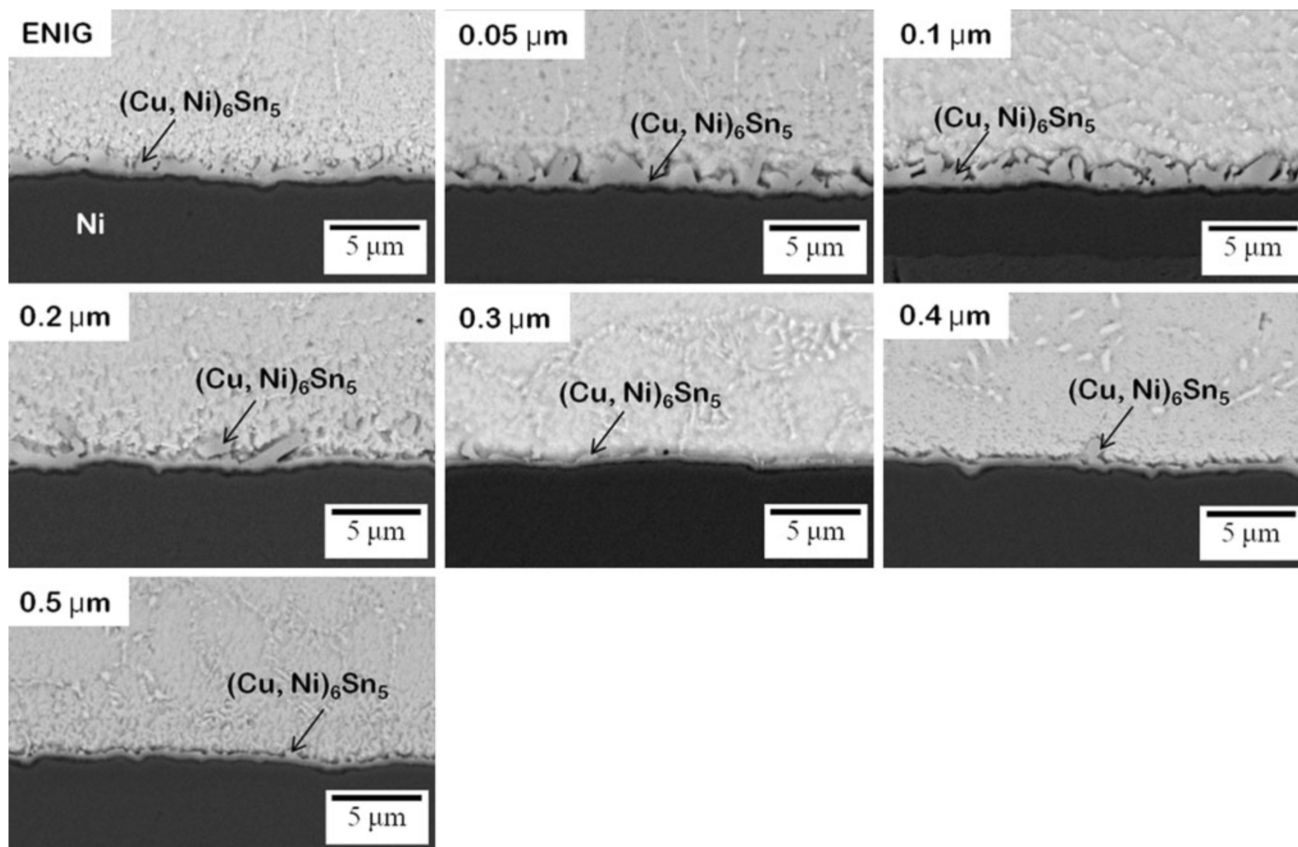

Fig. 10. BSE micrographs of the SAC/ENEPIG interfaces with different thicknesses of Pd reflowed at 260°C for holding time of 20 s.

Interfacial Reaction and Strengths of SAC/ENEPIG Solder Joints After Reflow at 260°C for 20 s

Figure 10 shows cross-sectional BSE micrographs of the SAC/ENEPIG interfacial microstructures with different Pd thicknesses after reflow at 260°C for 20 s. Contrary to Fig. 2, only a thin and continuous $(Cu,Ni)_6Sn_5$ layer formed in the solder interfaces. $(Pd,Ni)Sn_4$ phase was not observed at the SAC/ENEPIG interface in any sample. The average thickness of $(Cu,Ni)_6Sn_5$ and the shear strength measured under shear speed of 500 mm/s are plotted against Pd thickness in Fig. 11.

For Pd thickness of 0.05 μm or 0.1 μm, the thickness of the $(Cu,Ni)_6Sn_5$ increased compared with that formed at the SAC/ENIG interface. A similar trend has been reported in the interfacial reaction at the SAC/ENEPIG interface.[28] It was thought that the Pd layer addition resulted in accelerated IMC growth at an early reflow stage. However, the thickness of the $(Cu,Ni)_6Sn_5$ decreased gradually with Pd thickness. When a continuous $(Pd,Ni)Sn_4$ phase formed above the $(Cu,Ni)_6Sn_5$ IMC, the growth of $(Cu,Ni)_6Sn_5$ was delayed due to the diffusion barrier role of $(Pd,Ni)Sn_4$. Since the initially formed $(Pd,Ni)Sn_4$ on the $(Cu,Ni)_6Sn_5$ IMC layer already spalled off the $(Cu,Ni)_6Sn_5$ interface as the reflow holding time

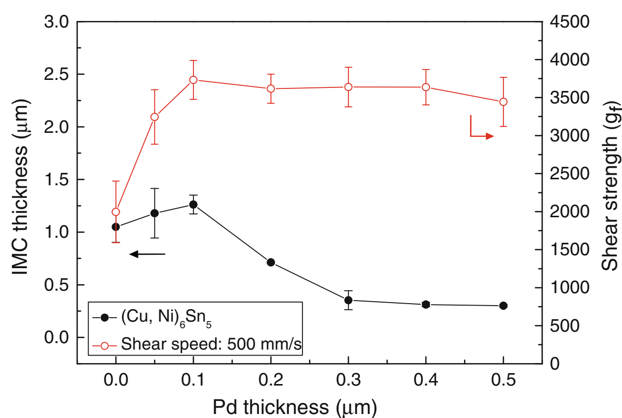

Fig. 11. $(Cu,Ni)_6Sn_5$ IMC thickness (solid circle) and SAC/ENEPIG shear strength (open circle) as functions of Pd thickness under shear speed of 500 mm/s after reflow at 260°C for 20 s.

increased, only $(Cu,Ni)_6Sn_5$ IMC remained at the solder/Ni(P) interface.

The mechanical strengths of the SAC/ENIG solder joints showed the lowest values among the tested samples. Compared with the SAC/ENIG solder joints, the insertion of a Pd layer between the Ni/Au bilayer improved the mechanical strengths of the solder joints. The interfacial strengths of SAC solder joints on ENEPIG were improved compared with

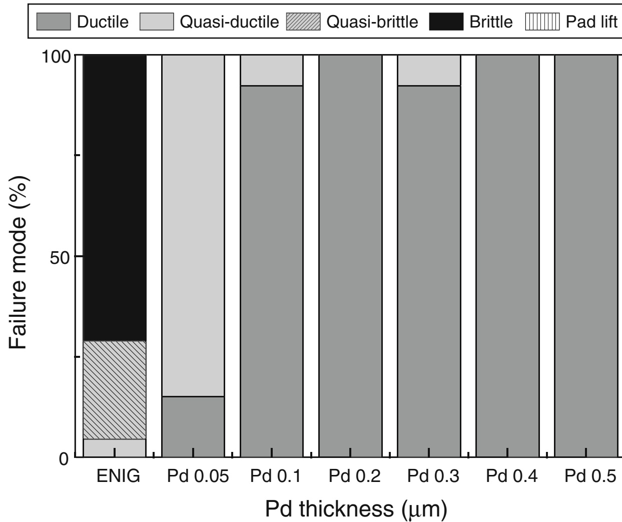

Fig. 12. Failure mode distribution after high-speed ball shear test of SAC/ENEPIG solder joints with various thicknesses of Pd under shear speed of 500 mm/s (reflow holding time: 20 s).

the solder joints without a Pd layer (ENIG). The mechanical strengths of the SAC/ENEPIG solder joints increased with Pd thickness and remained constant above 0.1 μm Pd thickness. Similar results also demonstrated that interfacial strength was increased by applying Pd thickness of 0.05 μm[16] or 0.1 μm to the ENEPIG surface finish.[7]

Failure mode distributions of the SAC/ENEPIG solder joints obtained at shear speed of 500 mm/s are shown in Fig. 12. At the SAC/ENIG solder joints, the dominant fracture mode was brittle failure, which is consistent with previous studies regarding the mechanical properties of SAC/ENIG solder joints.[7,32] A clear transition of the failure mode was observed from brittle mode in ENIG occurring at the $(Cu,Ni)_6Sn_5$/solder interface to quasiductile mode in ENEPIG with 0.05-μm-thick Pd, and then ductile mode in ENEPIG with Pd thickness of 0.1 μm or greater. When the reflow holding time was prolonged to 20 s, spalling of the $(Pd,Ni)Sn_4$ from the solder interfaces occurred, only $(Cu,Ni)_6Sn_5$ IMC remained at the SAC/Ni(P) interface, and the weak interface between $(Pd,Ni)Sn_4$ and $(Cu,Ni)_6Sn_5$ was not sustained. Thus, the main fractures during high-speed ball shear tests in the ENEPIG samples occurred predominantly in the solder region (ductile mode). It was confirmed that a decrease in shear strength was not observed, since fractures occurred primarily on the interior of the solder matrix rather than along the solder interfaces.

CONCLUSIONS

The effects of Pd thickness on interfacial microstructures and the mechanical strength of SAC/ENEPIG solder joints depend on the reflow conditions. At low reflow temperature and short reflow holding time (255°C for 5 s), the $(Pd,Ni)Sn_4$ phase was the predominant IMC above the residual Pd layer. As the reflow temperature and holding time increased, spalling of $(Pd,Ni)Sn_4$ into the solder matrix was accelerated, and $(Cu,Ni)_6Sn_5$ formed beneath the $(Pd,Ni)Sn_4$ layer at the solder interface. When the Pd thickness increased, the $(Pd,Ni)Sn_4$ phase became continuous and retarded the growth of $(Cu,Ni)_6Sn_5$ IMC by interrupting the interdiffusion of Sn and Cu (and Ni). In case of reflow conditions of 260°C for 5 s, a $(Pd,Ni)Sn_4/(Cu,Ni)_6Sn_5$ bilayer formed continuously at the solder interface as the Pd thickness increased. The formation of the $(Pd,Ni)Sn_4/(Cu,Ni)_6Sn_5$ structure was very poor with regard to the mechanical strength of the interface, deteriorating the reliability of the solder joints. On the other hand, only the $(Cu,Ni)_6Sn_5$ phase formed on the Ni-Sn-P layer at the SAC/ENEPIG interfaces as the Pd thickness increased since a continuous $(Pd,Ni)Sn_4$ layer separated from the solder interfaces for the reflow condition of 260°C for 20 s. Thus, no degradation of the interfacial strength of the SAC/ENEPIG solder joints was observed. The suitable range of Pd thickness in ENEPIG for application in Pb-free solder joint pads was determined to be 0.1 μm to 0.2 μm based on microstructure, mechanical strength, and failure mode.

ACKNOWLEDGEMENT

This work was supported by the National Research Foundation of Korea (NRF) Grant funded by the Korea Government (MEST) (No. 2011-0015735).

REFERENCES

1. A.J.G. Strandjord, S. Popelar, and C. Jauernig, *Microelectron. Reliab.* 42, 265 (2002).
2. D.K.W. Yee, L. Leung, and M. Bayes, *Proceeding of International Microsystems, Packaging, Assembly and Circuits Technology Conference, IMPACT* (2007).
3. K. Zeng, R. Stierman, D. Abbott, and M. Murtuza, *JOM* 58, 75 (2006).
4. P. Ratchev, S. Stoukatch, and B. Swinnen, *Microelectron. Reliab.* 46, 1315 (2006).
5. K. Johal, S. Lamprecht, and H. Roberts, *Proceeding of SMTA 9th Annual Pan Pacific Microelectronics Symposium* (2004).
6. Y. Oda, M. Kiso, S. Kurosaka, A. Okada, K. Kitajima, and S. Hashimoto, *Proceeding of International Microelectronics & Packaging Society, IMAPS* (2008).
7. W.H. Wu, C.S. Lin, S.H. Huang, and C.E. Ho, *J. Electron. Mater.* 39, 2387 (2010).
8. Y. Kim, J. Yoon, and S.-B. Jung, *12th International Conference on Electronics Materials and Packaging*, (2010), p. 153.
9. G. Ghosh, *J. Electron. Mater.* 28, 1238 (1999).
10. C.T. Lu, H.W. Tseng, C.H. Chang, T.S. Huang, and C.Y. Liu, *Appl. Phys. Lett.* 96, 232103 (2010).
11. Y.D. Jeon, Y.B. Lee, and Y.S. Choi, *Proceedings of Electronic Components and Technology Conference* (2006), p. 119.
12. C.H. Fu, L.Y. Hung, D.S. Jiang, Y.P. Wang, and C.S. Hsiao, *Proceedings of Microsystems Packaging Assembly and Circuits Technology Conference* (2007), p. 331.
13. JESD22-B117A, *Solder Ball Shear* (JEDEC Solid State Technology Association, 2006).
14. G. Ghosh, *Acta Mater.* 48, 3719 (2000).
15. S. Tanaka and M. Kajihara, *J. Alloy Compd.* 484, 273 (2009).

16. S.P. Peng, W.H. Wu, C.E. Ho, and Y.M. Huang, *J. Alloy Compd.* 493, 431 (2010).
17. S.C. Yang and C.R. Kao, *Proceedings of Electronic Components and Technology Conference* (2007), p. 1825.
18. H.K. Kim, K.N. Tu, and P.A. Totta, *Appl. Phys. Lett.* 68, 2204 (1996).
19. C.Y. Liu, H.K. Kim, K.N. Tu, and P.A. Totta, *Appl. Phys. Lett.* 69, 4014 (1996).
20. C.-E. Ho, S.-W. Lin, and Y.-C. Lin, *J. Alloy Compd.* 509, 7749 (2011).
21. K. Nogita and T. Nishimura, *Scripta Mater.* 59, 191 (2008).
22. W.T. Chen, C.E. Ho, and C.R. Kao, *J. Mater. Res.* 17, 263 (2002).
23. C.E. Ho, R.Y. Tsai, Y.L. Lin, and C.R. Kao, *J. Electron. Mater.* 31, 584 (2002).
24. J.W. Jang, D.R. Frear, T.Y. Lee, and K.N. Tu, *J. Appl. Phys.* 88, 6359 (2000).
25. Y.C. Lin and J.G. Duh, *Scripta Mater.* 54, 1661 (2006).
26. D.-H. Lee, B.-M, Chung, and J.-Y. Huh, *Proceedings of the 12th International Conference on Electronics Materials and Packaging* (Singapore, 2010), p. 153.
27. G.E. Dieter, *Mechanical Metallurgy* (New York: McGraw-Hill, 1988).
28. A. Nadai, *Theory of Flow and Fracture of Solids* (New York: McGraw-Hill, 1950).
29. F. Song, S.W.R. Lee, K. Newman, B. Sykes, and S. Clark, *Proceedings of Electronic Components and Technology Conference* (2007), p. 1504.
30. R. Darveaux and C. Reichman, *Proceedings of Electronic Components and Technology Conference* (2006), p. 283.
31. P.A. Kramer, J. Glazer, and J.W. Morris Jr., *Metall. Mater. Trans. A* 25, 1249 (1994).
32. C.E. Ho, W. Gierlotka, and S.W. Lin, *J. Mater. Res.* 25, 2078 (2010).